
PROFILE MONITORING VIA EIGENVECTOR PERTURBATION

Takayuki Iguchi

Department of Statistics, Florida State University

Andrés F. Barrientos

Department of Statistics, Florida State University

Eric Chicken

Department of Statistics, Florida State University

Debajyoti Sinha

Department of Statistics, Florida State University

June 1, 2022

ABSTRACT

Control charts are often used to monitor the quality characteristics of a process over time to ensure undesirable behavior is quickly detected. The escalating complexity of processes we wish to monitor spurs the need for more flexible control charts such as those used in profile monitoring. Additionally, designing a control chart that has an acceptable false alarm rate for a practitioner is a common challenge. Alarm fatigue can occur if the sampling rate is high (say, once a millisecond) and the control chart is calibrated to an average in-control run length (ARL_0) of 200 or 370 which is often done in the literature. As alarm fatigue may not just be an annoyance but result in detrimental effects to the quality of the product, control chart designers should seek to minimize the false alarm rate. Unfortunately, reducing the false alarm rate typically comes at the cost of detection delay or average out-of-control run length (ARL_1). Motivated by recent work on eigenvector perturbation theory, we develop a computationally fast control chart called the Eigenvector Perturbation Control Chart for nonparametric profile monitoring. The control chart monitors the l_2 perturbation of the leading eigenvector of a correlation matrix and requires only a sample of known in-control profiles to determine control limits. Through a simulation study we demonstrate that it is able to outperform its competition by achieving an ARL_1 close to or equal to 1 even when the control limits result in a large ARL_0 on the order of 10^6 . Additionally, non-zero false alarm rates with a change point after 10^4 in-control observations were only observed in scenarios that are either pathological or truly difficult for a correlation based monitoring scheme.

Keywords Profile Monitoring · Statistical Process Control · Eigenvector Perturbation · Alarm Fatigue

1 Introduction

Monitoring a process of interest over time to ensure it behaves as desired is a common task. The field of statistical process control (SPC) aims to solve this problem from a statistical perspective. The assumptions about the process of interest plays a key role in the development of monitoring methods, typically called control charts. The increasing complexity of processes of interest due to technological developments and automated data acquisition are driving the need for more flexible and general control charts. In addition, there are two common challenges in control chart design: reducing the false alarm rate and reducing the detection delay of undesired, or out-of-control, behavior of the underlying process.

The negative impacts of frequent false alarms include increased costs in determining if an alarm is warranted and a user losing confidence in a control chart thereby ignoring a true alarm. These problems are only exacerbated as the time between observations decreases which occurs with streaming data [37]. Control charts are typically calibrated to raise a false alarm on average after 200 or 370 in-control observations (also known as the in-control Average Run Length, or ARL_0). If the process needs to be monitored each millisecond, for example, the average time to signal would be 200 or 370 milliseconds under this type of calibration which is clearly undesirable. In hospital intensive care units, the rate of false alarms has detrimental effects on patient safety and the effectiveness of patient care [20]. Control limits

could be widened to reduce the false alarm rate (FAR), but doing so typically comes at the cost of fast detection of an out-of-control observation. In this paper, we aim to provide a nonparametric control chart for a general SPC task called profile monitoring and show empirically that it has the ability to achieve an extremely low false alarm rate without sacrificing much in detection delay.

In this paper, the observed quality characteristics (called profiles) y_i^t for $i \in \{1, \dots, n\}$ at time-point t are noisy observations of n discretely sampled values of a function f^t of the observed vector \mathbf{x}_i^t of a d dimensional explanatory variable. So, at each time t , observation y_i^t of each functional profile has mean $E[Y_i^t] = f^t(\mathbf{x}_i^t)$.

Our proposed control chart exploits two ideas:

- According to recent works in eigenvector perturbation theory including Morales-Jimenez et al. [28], the difference between the observed value of normalized leading eigenvector \mathbf{v}_1 of a sample correlation matrix \mathbf{R} and the normalized leading eigenvector $\tilde{\mathbf{v}}_1$ of $\mathbb{E}[\mathbf{R}]$ is very small (in l_2 norm).
- For a fixed set of predictors, the expected correlation matrix of a set of responses from w observed in-control profiles has rank one with leading eigenvector $\frac{1}{\sqrt{w}}\mathbf{1}$. If, however, if the responses come from a mix of in-control and out-of-control profiles, then $\mathbb{E}[\mathbf{R}]$ has 4 blocks partitioned structure (ignoring the diagonal) whose both eigenvectors being different from $\frac{1}{\sqrt{w}}\mathbf{1}$.

Therefore, if we obtain \mathbf{R} using responses from w in-control profiles, then $\|\mathbf{v}_1 - \frac{1}{\sqrt{w}}\mathbf{1}\|_2$ should be small, and if \mathbf{R} is obtained using responses from a mix of observed in-control and out-of-control profiles, then $\mathbf{v}_1 \not\approx \frac{1}{\sqrt{w}}\mathbf{1}$ and $\|\mathbf{v}_1 - \frac{1}{\sqrt{w}}\mathbf{1}\|_2$ should be large. Hence, we propose our control chart using this eigenvector perturbation. If $\|\mathbf{v}_1 - \frac{1}{\sqrt{w}}\mathbf{1}\|_2$ exceeds some control limit U , we claim at least one of the w observed profiles is out-of-control. To determine a control limit we combine a parametric bootstrap approach using a sample of m historical, known in-control profiles and an empirically useful approximation of the distribution of eigenvector perturbation.

Using this approach, we empirically demonstrate that our control chart achieves an ARL_0 even larger than 10^6 . Unsurprisingly, such a large ARL_0 results in low FAR even when the change-point occurs long after monitoring has begun (say after 10^4 in-control profiles have been observed). Typically, a control chart with such a large ARL_0 would suffer from a large detection delay. We show this phenomenon for the competitors of this control chart by slightly increasing the ARL_0 from 200 to 370 and observing a noticeable increase in ARL_1 for our competitors. So even if calibrating control limit to $ARL_0 > 10^6$ for the competing control charts are possible, they result in also large ARL_1 . Surprisingly, our proposed control chart is able to immediately detect an out-of-control process (i.e., $ARL_1 = 1$) even while maintaining $ARL_0 > 10^6$. Moreover, the proposed control chart is computationally fast, especially when compared to its competition. The combination of the extremely large ARL_0 , small ARL_1 , and computational speed allows this control chart to be applied to streaming data with good performance.

The paper is organized as follows. Section 2 provides a brief background on profile monitoring (especially in the nonlinear nonparametric case) and on eigenvector perturbation theory. Section 3 discusses the construction of the eigenvector perturbation control chart in more detail and provides the method for determining control limits. Section 4 covers the simulation study demonstrating the superiority of the eigenvector perturbation control chart in specificity, sensitivity, and computational speed among other nonlinear nonparametric profile monitoring methods. Section 4 also discusses conditions in which the performance of the eigenvector perturbation control chart begins to degrade. Section 5 concludes the paper with a discussion and areas of future work.

2 Background

Here, we describe the relevant literature on profile monitoring in section 2.1 and provide a brief introduction into eigenvector perturbation in section 2.2.

2.1 Profile Monitoring

The major aim of SPC is the accurate sequential detection of changes in quality characteristics. Typically, these quality characteristics should reflect desired, "in-control" conditions of some monitored process, and deviations from these desired conditions, termed "out-of-control", should be quickly and accurately identified. One of the common assumptions about the data generating process is the quality characteristics being generated by noise contaminated, discretely sampled functions called profiles. The model of profiles considered in this paper is

$$y_i^t = f^t(\mathbf{x}_i^t) + \epsilon_i^t, \quad i \in [n] \quad (1)$$

for each time-point t where $y_i^t \in \mathbb{R}$ is the scalar value of the quality characteristic at discretely sampled points $i \in [n] = \{1, \dots, n\}$, $\mathbf{x}_i^t \in \mathbb{R}^d$ is the vector of the corresponding values of d dimensional explanatory variables, and the error ϵ_i^t represents the independent and identically distributed mean-zero random noise inherently associated with the process. In this setting, we assume the random predictors $\{\mathbf{x}_i^t\}$ to be independent, identically distributed, and, additionally, independent of the errors ϵ_i^t . For the remainder of the paper, by the abuse of notation, we denote f to be the functional relationship for the in-control profile (or the in-control function) and f^t to be the functional relationship between the responses and predictors at time t . Additionally, we let $t \in \{-(m-1), \dots, 0\}$ denote the time steps of m historical in-control profiles with known $f^0 = \dots = f^{m-1} = f$. The goal of profile monitoring is to accurately detect if any of the f^1, \dots, f^T are different from f given (y_i^t, \mathbf{x}_i^t) for $i \in [n]$ and $t = -(m-1), \dots, T$.

Profile monitoring has been applied in many settings including semiconductor manufacturing [13], monitoring a stamping operation force [21], developing artificial sweeteners [22], evaluating the curvature of a mechanical component [8], and automobile engine testing [2]. Like other SPC methods, profile monitoring typically consists of two steps: Phase I and Phase II. To accurately distinguish an in-control process from some other unknown out-of-control process, a Phase I analysis aims to define a notion of "in-control" via modeling the desired in-control performance of a process using a retrospective analysis of available historical data. Using the model for an in-control process obtained from Phase I, the goal of a Phase II analysis is to detect deviations from an in-control process in an online fashion using observations (y_i^t, \mathbf{x}_i^t) of quality characteristics collected sequentially over time t .

Ideally, a good profile monitoring algorithm should not wrongly claim an in-control process at any time-point to be as out-of-control, yet should signal a process to be out-of-control soon after it becomes out-of-control. Thus, the performance of a profile monitoring method typically is evaluated based on the mean time until a change is detected in an out-of-control process (ARL_1), and some measure of how often false alarms occur when the process is in-control. One such measure is the mean time until a false alarm, called the average in-control run length (ARL_0). We can define a false alarm rate (FAR) as the probability that an alarm is a false alarm at some point in time when an in-control process is detected as out-of-control. Typically, control charts are used to detect a deviation from in-control conditions. A control chart determines if a process is in-control (or out-of-control) if a particular monitoring statistic lies inside (or outside) of an interval whose endpoints are called control limits. Akin to traditional hypothesis testing where a significance level is specified prior to the implementation of analysis, the control limits are calibrated to ensure a desired ARL_0 in Phase I prior to commencing any online monitoring at Phase II.

In the profile monitoring setting, the monitoring statistic is commonly a summary of a fitted (estimated) profile. The choice of monitoring statistics is usually based on a set of assumptions about the underlying structure of the profile and the corresponding method for estimation of f^t in (1). Performance of the parametric approaches for estimating f^t depends on the parametric assumption on f^t being correct. Poor performance can occur if the parametric assumption on unknown f^t is incorrect or misspecified. Additionally, a practitioner may only have access to quality data under in-control conditions and may not have any parametric model for out-of-control profiles. As such, we consider nonparametric profile monitoring. Further, in an attempt to be as general as possible with our assumptions, we allow f^t to be nonlinear.

Extensive work has been done on nonlinear nonparametric profile monitoring using a univariate predictor (e.g., [36], [40], [5], [3], [29], [7], [16], [27], [14], [38], [6], [33]). The literature on multivariate predictors is less extensive and can be categorized by the estimation procedures for f^t , the choice of monitoring statistic, the calibration method for control limits, and whether the predictors vary over different time-points. An overview of nonlinear nonparametric profile monitoring procedures using multiple predictors is provided in Table 1.

The methods of Hung et al. [17] and Li et al. [26] use support-vector regression (SVR), but with different monitoring statistics. The method of [17] claims a profile at time t to be out of control if \hat{f}^t lies outside a moving block bootstrap confidence region for \hat{f}^t . The procedure of [26] uses a nonparametric EWMA control chart from Hackl and Ledolter [15] on the Williams et al. [36] nonparametric statistics calculated on the residuals of a support vector regression on a profile. Both approaches from [17] and [26] rely on ranking a monitoring statistic against a set of historical values. Although robust to possible outliers, a rank-based statistic may not have good power (i.e., poor/large ARL_1) because they do not effectively use the underlying model of f^t in (1). The method by Iguchi et al. [19] uses a single-index model (SIM) of Kuchibhotla and Patra [23, 24] to fit a profile and use an l_2 -based statistic on the index parameters. Although the existing SIM based approach of Iguchi et al. results in a competitive FAR and low ARL_1 , its performance comes at the cost of slow computational speed. None of these methods simultaneously enjoy a low FAR, a small ARL_1 , and fast computational speed. Our proposed eigenvector perturbation control chart enjoys all of these desirable properties for a large collection of combinations of in-control and out-of-control profiles. The associated monitoring scheme is detailed in Section 3.2.

The low FAR of the eigenvector perturbation control chart leverages a quick method of calibrating to a large, but unknown ARL_0 . All existing approaches for nonlinear nonparametric profile monitoring cannot simultaneously

Model for f^t	Detection method	Control Limit	Predictors	Year	Source
SVR	Fitted model lies in a confidence region	Confidence level for confidence region. No ARL_0 calibration	Fixed or Random	2012	Hung et al. [17]
	EWMA on the rank of observed Williams et al. [36] statistics among a historical in-control set	Monte carlo using known f	Fixed for all t	2019	Li et al. [26]
SIM	l_2 based statistic of SIM index parameter	Monte carlo using known f	Random	2021	Iguchi et al. [19]
None	Eigenvector perturbation on noisy responses	Quantile of parametric bootstrapped monitoring statistics	Fixed for all t	This paper	§3

Table 1: Overview of nonlinear nonparametric (or semiparametric) profile monitoring methods with multiple predictors

calibrate to a large ARL_0 and ensure good performance in terms of FAR and ARL_1 . While obtaining competitive FAR and ARL_1 , the approaches of Iguchi et al. and Li et al. require calibration of control limit through a Monte Carlo approach. Due to the sequential nature of the profile monitoring problem, calibrating to a desired ARL_0 requires each trial to have a larger than desired ARL_0 . For example, if the discrete time-point of a false alarm follows a geometric distribution (say with $p = 1/ARL_0$), then the variance of run length is $O(ARL_0^2)$. Therefore, calibrating control limits to large ARL_0 (say $ARL_0 > 10^6$) through a Monte Carlo approach, is infeasible. Such an approach is not only computationally intensive, but also requires explicit knowledge of f making the Phase I approach parametric despite the nonparametric approach for Phase II. The eigenvector perturbation control chart avoids the Monte Carlo approach and can quickly find a control limit that achieves a large, but unknown ARL_0 through a bootstrapping strategy. Our proposed method to calibrate control limits for the eigenvector perturbation control chart is detailed in Section 3.3.

2.2 Eigenvector Perturbation

Monitoring eigenspaces is a popular technique in the change-point detection and SPC literature. For example, the procedure by Wang and Samworth [34] applies change-point detection of a univariate projection of high dimensional time-series to a left singular vector of a matrix containing information about the time series being monitored. Principal component analysis type methods have been explored by [30, 32, 35] and others. To the best of our knowledge, application of l_2 distance based perturbation of eigenvector is new to the profile monitoring and the SPC literature. To define this eigenvector perturbation more explicitly, let us define $\mathbf{M} = \widetilde{\mathbf{M}} + \mathbf{E}$, where $\widetilde{\mathbf{M}} \in \mathbb{R}^{w \times w}$ is symmetric and fixed and \mathbf{E} is some random perturbation matrix. Let \mathbf{v} and $\tilde{\mathbf{v}}$ respectively be the leading eigenvectors of \mathbf{M} and $\widetilde{\mathbf{M}}$ with corresponding eigenvalues λ and $\tilde{\lambda}$. The goal is to answer the question: “*Under certain assumptions of $\widetilde{\mathbf{M}}$ and \mathbf{E} , how ‘far’ can the j th leading eigenvector \mathbf{M} be from the j th leading eigenvector of $\widetilde{\mathbf{M}}$?*” To employ eigenvector perturbation to profile monitoring, we must do two things. First, we must define a matrix \mathbf{M} that reflects in-control conditions, and secondly we must set a control limit based on either the possible values of \mathbf{E} or a sample of eigenvector perturbations under in-control conditions.

For the first task, we draw inspiration from the work of Morales-Jimenez et al. [28] on asymptotics of the eigenvalues and eigenvectors of the sample correlation matrix under a special case of spiked covariance model where some eigenvalues of the population covariance (correlation) matrix are well separated from the rest such that the population correlation matrix can be expressed as a block diagonal matrix with diagonal blocks Γ_{spike} and \mathbf{I} for some small sized correlation matrix Γ_{spike} with eigenvectors corresponding to this “spike” expressed as $[\mathbf{v}^\top, \mathbf{0}^\top]^\top$. Under this model, the results in [28] showed that the asymptotic variance of $\langle \hat{\mathbf{v}}, \mathbf{v} \rangle^2$ is smaller for the sample correlation matrix than for the sample covariance matrix. The results from [28] can be translated from a statement about inner products to a statement about the angle θ between two eigenvectors which can again be translated into a statement regarding their euclidean distance (through say the law of cosines). Although the profiles in this paper do not follow the specific data model in [28], the covariance matrix of the responses from w in-control profiles do follow a spiked covariance model (specifically, with covariance $\text{Var}(f)\mathbf{1}\mathbf{1}^\top + \sigma^2\mathbf{I}$ where $\text{Var}(f)$ is computed with respect to the random predictors) which results in one dominant eigenvalue and all other eigenvalues small and equal. Due to the similarity of the eigenspace of the correlation matrix under our consideration with the eigenspace of the correlation matrix in [28], we consider the l_2 perturbation of the sample correlation matrix. The construction of our eigenvector perturbation based control chart is discussed in Section 3.2.

We now discuss the background relevant to our second task of adopting eigenvector perturbation for profile monitoring. For the needed control limit of the eigenvector perturbation, the literature provides nonasymptotic bounds on how large this can be depending on the properties of $\tilde{\mathbf{M}}$ and \mathbf{E} . An important example is in Davis-Kahan $\sin(\theta)$ Theorem [9] which provides an upper bound of the sine of the angle between $\tilde{\mathbf{v}}_j$ and \mathbf{v}_j . Using some trigonometry, the $\sin(\theta)$ as a measure of dissimilarity between $\tilde{\mathbf{v}}_j$ and \mathbf{v}_j is analogous to $\|\tilde{\mathbf{v}}_j - \mathbf{v}_j\|_2$. Therefore, an application of the law of cosines can translate any bound of $\sin(\theta)$ into a bound on l_2 perturbation. In the past decade, there has been growing literature on improving these nonasymptotic bounds on l_2 perturbation [4, 31, 39] and very recently bounds on l_∞ perturbation [4, 10, 11]. Nearly all of these bounds are of the form $\mathcal{O}(\|\mathbf{E}\|)$ divided by some measure of an eigengap. For example, a reformulation of the Davis-Kahan bound by Yu et al. [39] is $\sin \theta_j \leq \|\mathbf{E}\|_2 / \min(|\lambda_{j-1} - \tilde{\lambda}_j|, |\lambda_{j+1} - \tilde{\lambda}_j|)$.

If the aim is to reduce the probability of false alarms, setting a control limit to one of these bounds may achieve nearly zero probability of false alarms. Unfortunately, this bound like many other bounds from the eigenvector perturbation literature is not tight enough to be useful as practical control limits because it results in low or nonexistent sensitivity. There are other bounds found in the literature claiming to be rate-optimal, but these bounds typically involve latent constants which are either too large to be useful for obtaining practical control limit or difficult to estimate from data. To construct our control limits in Section 3.2, we leverage knowledge that a nonasymptotic bound exists for the eigenvector perturbation and that the perturbation is typically small for a sample correlation matrix.

3 Methodology

In this section we describe the proposed control chart. Section 3.1 details the specific profile monitoring problem we consider under the a change-point framework. Section 3.2 details the construction of the proposed control chart, and section 3.3 describes the procedure for obtaining a control limit based solely on a set of known, in-control profiles.

3.1 Change-point framework

The underlying model

$$y_i^t = \begin{cases} f(\mathbf{x}_i^t) + \epsilon_i^t, & t \leq \tau \\ h(\mathbf{x}_i^t) + \epsilon_i^t, & \text{else} \end{cases} \quad i \in [n] \quad (2)$$

of profile $\{(\mathbf{x}_i^t, y_i^t) : i \in [n]\}$ at time t is a special case of model in (1), where f denotes the in-control functional relationship between the response y and the explanatory variables \mathbf{x} , h is some other unknown function defining the out-of-control state, and τ is the unknown time of change-point. In this paper, we consider h of the form $h = \nu f + (1 - \nu)g$ for $\nu \in \mathbb{R}$ where the unknown g is called the out-of-control forcing function. Assume that the errors in equation (2) are independent and identically distributed with zero mean and constant variance σ^2 . For notational convenience, let $\mathbf{X}^t \in \mathbb{R}^{n \times d}$ and $\mathbf{y}^t \in \mathbb{R}^n$ denote the matrix of the explanatory variables and the vector of observed responses at time t . Similarly, let \mathbf{X}^t and \mathbf{y}^t for $t = 1 - m, \dots, 0$ denote m noise perturbed, known in-control profiles taken from historical data or expert knowledge. For the purposes of this paper, we further restrict the explanatory variables to be fixed for all time-points (i.e., $\mathbf{X}^t = \mathbf{X}$ for all t), though in reality this \mathbf{X} may be chosen randomly.

The goal is to correctly determine from T observed profiles if a process at time T is out-of-control from m known in-control profiles from historical data. That is, we wish to test the following hypothesis:

$$H_0 : \tau \geq T \text{ versus } H_a : \tau < T, \quad (3)$$

where H_0 is equivalent to $f = f^1 = \dots = f^T$ for f^t in (1). An ideal change point detection method should be able to detect a profile being out-of-control whenever T is close to, but greater than, τ .

3.2 Constructing the eigenvector perturbation control chart

Consider the responses from w observed profiles $\{\mathbf{y}^t\}_{t=t_0}^{w+t_0}$ for some t_0 , and define $\mathbf{R} \in \mathbb{R}^{w \times w}$ to be the sample correlation matrix of these responses with leading eigenvector \mathbf{v} . In the eigenvector perturbation setup, we can consider either the population correlation matrix Γ or the expected sample correlation matrix $\mathbb{E}[\mathbf{R}]$ to be the fixed non-random matrix. Note these are not the same as the sample correlation matrix \mathbf{R} is a biased estimator of Γ (see [12], Example 2.4 in [25]). Fortunately, both have the same structure and differ only by a constant in the off-diagonal entries. We choose $\mathbb{E}[\mathbf{R}]$ as the unperturbed matrix with leading eigenvector $\tilde{\mathbf{v}}$ for the rest of the paper and define our perturbation matrix \mathbf{E} such that $\mathbf{R} = \mathbb{E}[\mathbf{R}] + \mathbf{E}$.

If all w profiles are all in-control, then off-diagonal entries of $\mathbb{E}[\mathbf{R}]$ are identical implying $\tilde{\mathbf{v}} = \frac{1}{\sqrt{w}}\mathbf{1}$. Now consider the sample correlation matrix \mathbf{R} for k_1^* in-control profiles and $k_2^* = w - k_1^*$ out-of-control profiles with γ_1, γ_2 and

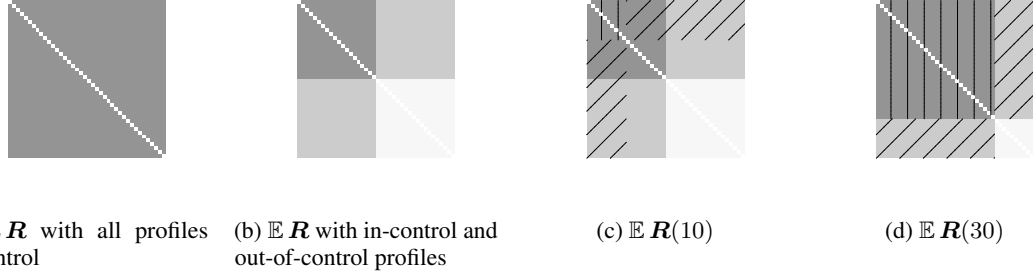


Figure 1: A visualization of correlation matrices. In (b)-(d), $w = 40$, $\tau = 20$, $T = 40$. The regions shaded with vertical lines reflect the entries substituted from the correlation matrix obtained from the historical in-control profiles. The regions shaded with diagonal lines correspond to the entries that need to be computed due to substituting k_1 of the oldest observed profiles with historical in-control profiles.

$\gamma_{12} = \gamma_{21}$ being the expected sample correlations $\mathbb{E}[\hat{\rho}]$ respectively between two in-control profiles, two out-of-control profiles, and one in-control and other out-of-control profile. Then $\mathbb{E}[\mathbf{R}]$ exhibits a block diagonal structure (aside from the diagonals) of the following form

$$\mathbb{E}[\mathbf{R}] = \gamma_{12}\mathbf{J} + (\gamma_1 - \gamma_{12})\mathbf{J}_{11} + (\gamma_2 - \gamma_{12})\mathbf{J}_{22} + (1 - \gamma_1)\text{diag}(\mathbf{u}_1^*) + (1 - \gamma_2)\text{diag}(\mathbf{u}_2^*) ,$$

where \mathbf{e}_l corresponds to the l th standard basis vector, $\mathbf{u}_1^* = \sum_{l=1}^{k_1^*} \mathbf{e}_l$, $\mathbf{u}_2^* = \sum_{l=k_1^*+1}^w \mathbf{e}_l$, and \mathbf{J} is a unit matrix, and each of $\mathbf{J}_{ll} = \mathbf{u}_l^* \mathbf{u}_l^{*\top}$ for $l = 1, 2$ is a block diagonal matrix with one unit matrix in the diagonal and rest zero matrices. Figure 1 provides a visualization of $\mathbb{E}[\mathbf{R}]$ under a scenario when all w profiles are in-control and other when only $k_1^* < w$ are in-control profiles. As the row sums of $\mathbb{E}[\mathbf{R}]$ for the first k_1^* rows are the same (the same is true for the last k_2^* rows), $\tilde{\mathbf{v}} \propto \xi^* \mathbf{u}_1^* + \mathbf{u}_2^*$ in this scenario for some constant ξ^* .

Now we leverage the differences between the leading eigenvectors under the in-control scenario and under the scenario with a mix of in-control and out-of-control profiles to create our monitoring statistic. Unlike under the in-control condition when $\|\mathbf{v} - \frac{1}{\sqrt{w}}\mathbf{1}\|_2$ should be small, \mathbf{v} should be very different from $\frac{1}{\sqrt{w}}\mathbf{1}$ when w profiles include at least one out-of-control profile because \mathbf{v} is close to a normalized version of $\xi^* \mathbf{u}_1^* + \mathbf{u}_2^*$ in this setting. Therefore, in this setting, we expect our chosen monitoring statistics $\|\mathbf{v} - \frac{1}{\sqrt{w}}\mathbf{1}\|_2$ to be large. The practical considerations for implementing this setup are following: (1) any algorithm that needs the computation of correlation matrix at every monitoring time-point has a high computational cost of order $O(w^2n)$; (2) accounting for the possible failure of the control chart to correctly flag a profile as being out-of-control by time T beyond time of change τ ; (3) specifying the procedure to compute the leading eigenvector of \mathbf{R} .

To address the first issue, our method's computational cost is $O(wn)$ because we need only update one row and column of the correlation matrix at each time step as last $w - 1$ rows and columns of \mathbf{R} at time $T - 1$ are the first $w - 1$ rows and columns of \mathbf{R} at time T .

Regarding the second issue, with the current procedure, all w profiles considered would be out-of-control at time $\tau + w$, and the control chart no longer would be able to detect an out-of-control profile as this scenario looks identical to the one where all w profiles are in-control. To mitigate this issue, we can sample without replacement k_1 of the m historical, in-control profiles to replace the $k_1 > 0$ oldest profiles of the w profiles being considered. Doing so guarantees an in-control reference frame with which to compare an out-of-control profile. Assuming \mathbf{R} has already been computed for a set of w profiles at time T , replacing k_1 of the oldest observed profiles modifies the sample correlation matrix. Denote $\mathbf{R}(k_1)$ be such a correlation matrix derived from \mathbf{R} through this replacement procedure and let $\mathbf{v}(k_1)$ and $\tilde{\mathbf{v}}(k_1)$ be the leading eigenvectors of $\mathbf{R}(k_1)$ and $\mathbb{E}[\mathbf{R}(k_1)]$, respectively. Figure 1 provides a visualization for two such instances of $\mathbb{E}[\mathbf{R}(k_1)]$. As the notation suggests, $\mathbf{v}(k_1)$ is dependent on k_1 . To see this, consider all w of the profiles to be out-of-control, so the only in-control profiles included in $\mathbf{R}(k_1)$ are the historical profiles. Then $\tilde{\mathbf{v}}(k_1) \propto \xi(k_1) \mathbf{u}_1 + \mathbf{u}_2$ where

$$\xi(k_1) = \frac{(k_1 - 1)\gamma_1 - (k_2 - 1)\gamma_2 \pm \sqrt{((k_1 - 1)\gamma_1 - (k_2 - 1)\gamma_2)^2 + 4k_1 k_2 \gamma_{12}^2}}{2k_1 \gamma_{12}},$$

and $k_2 = w - k_1$, $\mathbf{u}_1 = \sum_{i=1}^{k_1} \mathbf{e}_i$, $\mathbf{u}_2 = \sum_{i=k_1+1}^m \mathbf{e}_i$. The technical details for this derivation are in the supplementary materials. As $\tilde{\mathbf{v}}(k_1)$ is a function of k_1 , $\mathbf{v}(k_1)$ is also a function of k_1 . This implies the monitoring statistic $\|\mathbf{v}(k_1) -$

$\frac{1}{\sqrt{w}}\mathbf{1}||_2$ is also a function of k_1 . So a choice of k_1 is required, but the values of γ_{12} and γ_2 are not known before monitoring. Therefore, k_1 cannot be chosen to maximize the difference between a normalized $\xi(k_1)\mathbf{u}_1 + \mathbf{u}_2$ and $\frac{1}{\sqrt{w}}\mathbf{1}$. We choose instead to select L , evenly spaced values of k_1 (say $K = \{1, \lfloor \frac{w}{L} \rfloor, 2 \lfloor \frac{w}{L} \rfloor, \dots, (L-2) \lfloor \frac{w}{L} \rfloor, w-1\}$), and use $\max_{k_1 \in K} ||\mathbf{v}(k_1) - \frac{1}{\sqrt{w}}\mathbf{1}||_2$ as the monitoring statistic.

Algorithm 1: Modified Power Iteration Detector (adapted from Iguchi et al. [18])

```

Given: - Symmetric matrix  $M \in \mathbb{R}^{w \times w}$ 
      - Unit eigenvector  $\tilde{\mathbf{v}} \in \mathbb{R}^w$ 
      - Tolerance:  $\zeta > 0$ 
Do:
Draw  $\mathbf{q}$  uniformly at random from the unit sphere in  $\mathbb{R}^w$ 
while TRUE
    if  $|\mathbf{q}^\top M \mathbf{q}| > |\tilde{\mathbf{v}}^\top M \tilde{\mathbf{v}}|$  ## confirm  $\tilde{\mathbf{v}}$  is not the leading eigenvector of  $M$ 
        return( $\mathbf{q}$ )
        break
    else if  $(\tilde{\mathbf{v}}^\top \mathbf{q})^2 \geq 1 - \zeta$  ##  $\tilde{\mathbf{v}}$  is sufficiently close to the leading eigenvector of  $M$ 
        return( $\mathbf{q}$ )
        break
    end
     $\mathbf{q} = M\mathbf{q}/||M\mathbf{q}||_2$ 
end

```

Algorithm 2: Eigenvector Perturbation Control Chart

```

Given: - Historical data:  $\mathbf{X}^t, \mathbf{y}^t$  where  $\mathbf{y}^t \in \mathbb{R}^n$ ,  $\mathbf{X}^t \in \mathbb{R}^{n \times p}$ ,  $t \in \{1-m, \dots, 0\}$ 
      - Upper control limit:  $U > 0$ 
      - A nonempty  $K \subset [w-1]$ 
      - Tolerance for power iteration detector:  $\zeta$ 
      - Window size:  $w \leq m$ 
Do:
Compute the sample correlation matrix  $\mathbf{R}^* \in \mathbb{R}^{m \times m}$  of the historical profiles.
Set  $\mathbf{R}$  to be the last  $w$  columns and rows of  $\mathbf{R}^*$ 
 $S = -1$ ;  $T = 1$ 
#Conduct process monitoring
while  $S < U$ 
    Observe  $\mathbf{y}^T \in \mathbb{R}^n$ 
    Update  $\mathbf{R}$  to reflect correlations of  $\{\mathbf{y}^{T-w+1}, \dots, \mathbf{y}^T\}$ 
    for every  $k_1$  in  $K$ 
         $\mathcal{I} = [m]$ 
        if  $T < w - k_1$ 
             $\mathcal{I} = [m - w + k_1 + T]$ 
        Sample  $k_1$  indices  $j_1, \dots, j_{k_1}$  from  $\mathcal{I}$  without replacement
         $\mathbf{R}(k_1) = \mathbf{R}$ 
        Replace the first  $k_1$  rows/columns of  $\mathbf{R}(k_1)$  with the  $j_1, \dots, j_{k_1}$  rows/columns of  $\mathbf{R}^*$ 
         $\mathbf{v}(k_1) = \text{modified\_power\_iteration\_detector}(\mathbf{R}(k_1), \frac{1}{\sqrt{w}}\mathbf{1}, \zeta)$ 
     $S = \max_{k_1 \in K} ||\mathbf{v}(k_1) - \frac{1}{\sqrt{w}}\mathbf{1}||_2$ 
    if  $S > U$ 
        claim change point occurred
    else
         $T = T + 1$ 
    end
end

```

The last computational consideration we must address is the computation of the leading eigenvector \mathbf{v} of \mathbf{R} . Power iteration is a simple choice for computing the leading eigenvector of a symmetric matrix. Typically, the main concern in

using power iteration is the possibility of slow convergence. We claim the dominance of the leading eigenvalue of \mathbf{R} over the rest of the eigenvalues results in fast convergence. Power iteration on \mathbf{R} converges geometrically with ratio λ_2/λ_1 , so slow convergence becomes an issue if $\lambda_2/\lambda_1 \approx 1$ (see §5.2 of [1]). As the eigenvalues of \mathbf{R} should not deviate greatly from the eigenvalues of $\mathbb{E} \mathbf{R}$, we can use $\tilde{\lambda}_2/\tilde{\lambda}_1$ to approximate convergence of power iteration on \mathbf{R} . It can be shown $\tilde{\lambda}_1 = 1 + \gamma_1(w-1)$ and $\tilde{\lambda}_2 = \dots = \tilde{\lambda}_w = 1 - \gamma_1$. Therefore, $\tilde{\lambda}_2/\tilde{\lambda}_1 = \left(\frac{1+\gamma_1(w-1)}{1-\gamma_1}\right)^{-1} = \left(\frac{1}{1-\gamma_1} + \frac{\gamma_1}{1-\gamma_1}(w-1)\right)^{-1}$ which is well separated from 1 if either w is large or γ_1 is not too small. Note γ_1 is close to zero only if the in-control profile is difficult to distinguish from the noise (e.g., $\text{Var}(f) \leq \sigma^2$). We assume the in-control function f is sufficiently distinguishable from the noise, so we conclude that power iteration should converge reasonably quickly. Leveraging \mathbf{v} being close to $\frac{1}{\sqrt{w}}\mathbf{1}$ under in-control conditions, we adopt a modified version of power iteration from Iguchi et al. [18] detailed in Algorithm 1 which provides an early stopping rule when it becomes evident that the leading eigenvector is not $\frac{1}{\sqrt{w}}\mathbf{1}$. We combine all of the aforementioned modifications to the original monitoring scheme as detailed in Algorithm 2.

3.3 Determining control limits

To employ a control chart for eigenvector perturbation, we need an upper control limit U such that if the perturbation exceeds U , we claim one of the w observed profiles is out-of-control. A candidate for a control limit could be to use one the nonasymptotic bounds on eigenvector perturbation in the literature. Assuming we knew $\|\mathbf{E}\|$ and γ_1 under in-control conditions or had a good estimate of these quantities, the monitoring statistic would be guaranteed never to exceed the bound under in-control conditions. Using rate-optimal bounds found in the literature as control limits pose a problem: they have hidden constants which need to be found in order to obtain a control limit. These hidden constants can be unnecessarily large destroying any chance at detection of an out-of-control profile. Another method is required to determine control limits, and we use the existence of these bounds to motivate our choice of control limit.

Assume we have access to a large sample of eigenvector perturbations p_1, \dots, p_N under the in-control condition to inform our control limit. We know these perturbations have a finite upper bound, and we can reasonably believe the eigenvector perturbation has small variance based on empirical observations and the result regarding the remarkably small fluctuations of eigenvectors of the correlation matrix under a spiked covariance model from [28]. That is, the perturbations lie in $(0, C]$ with C small. As C is unknown, good choices of U satisfy either $U = C + c'$ for some very small $c' > 0$ or in the case where $U < C$, $P(\|\mathbf{v} - \frac{1}{\sqrt{w}}\mathbf{1}\|_2 < U) = 1 - c$ for some small $c > 0$. In the first case, we achieve zero false alarms, and in the second case, the false alarm rate is controlled by the choice of c . If we approximate $P(\|\mathbf{v} - \frac{1}{\sqrt{w}}\mathbf{1}\|_2 < U)$ with some distribution function F supported on $[0, \infty)$ whose probability density function has a light tail, then we can set U to be a large quantile for the distribution F (i.e., $F(U) = 1 - c$). In the worst case, we obtain performance similar when $U < C$ and $P(\|\mathbf{v} - \frac{1}{\sqrt{w}}\mathbf{1}\|_2 < U) = 1 - c$ where the false alarm rate can be controlled. In the best case, we get a control limit $U > C$ due to F having infinite support and because the density corresponding to F has a light tail, $U - C$ is small. As a normal distribution has a light tail, we fit a normal distribution to p_1, \dots, p_N using unbiased estimates for the mean and variance, and set U to be a large quantile of this fitted normal.

The above procedure relies on having a large sample size N of eigenvector perturbations from the in-control condition. We leverage predictors being fixed for all t to perform a parametric bootstrap. The procedure for this parametric bootstrap is outlined below for large values of N and N_0 with $N_0 \gg N$.

1. Obtain an estimate for f using $\widehat{f(\mathbf{X})} = \frac{1}{m} \sum_{t=1-m}^0 \mathbf{y}^t$, and use it to estimate the variance of the noise: $\hat{\sigma}^2 = \frac{1}{n(m-1)} \sum_{i=1}^n \sum_{t=1-m}^0 (\mathbf{y}_i^t - \widehat{f(\mathbf{X})}_i)^2$.
2. Compute $\mathbf{y}_*^s = \widehat{f(\mathbf{X})} + \boldsymbol{\epsilon}_*^s$ for all $s \in [N_0]$ where $\boldsymbol{\epsilon}_*^s \sim N(0, \hat{\sigma}^2 \mathbf{I})$.
3. For every $l \in [N]$, compute a sample correlation matrix \mathbf{R}_l using w of the \mathbf{y}_*^s sampling without replacement.
4. Compute $S_l = \max_{k_1 \in K} \|\mathbf{v}(k_1) - \frac{1}{\sqrt{w}}\mathbf{1}\|_2$ as in Algorithm 2 for every bootstrapped correlation matrix \mathbf{R}_l .
5. Using a small $c > 0$, set $U = F(1 - c; \hat{\mu}_S, \hat{\sigma}_S^2)$ where F is a normal distribution function for with mean $\hat{\mu}_S$ and variance $\hat{\sigma}_S^2$ and where these estimates are the typical unbiased estimators for the mean and variance of the $\{S_l\}_{l \in [N]}$ in the previous step.

4 Simulations

In this section, we detail two simulation studies and their results. The first simulation study compares the proposed eigenvector perturbation control chart against other nonparametric and semiparametric profile monitoring procedures

Factor	Levels	
In-control & out-of-control functions	$f(\mathbf{x}) = 1 + 3x_1 + 2x_2 + x_3$	$h(\mathbf{x}) = \nu f(\mathbf{x}) + (1 - \nu) \sin(2\pi x_1 x_2)$
	$f(\mathbf{x}) = \frac{4}{9} (3x_1 + 2x_2 + x_3)^2$	$h(\mathbf{x}) = \nu f(\mathbf{x}) + (1 - \nu) 5 \sin(2\pi x_1 x_2)$
	$f(\mathbf{x}) = 1 + 3x_1 + 2x_2 + x_3$	$h(\mathbf{x}) = \nu f(\mathbf{x}) + (1 - \nu) 25 x_1 - 0.5 e^{-x_2} I(x_3 > 0.5)$
	$f(\mathbf{x}) = \frac{4}{9} (3x_1 + 2x_2 + x_3)^2$	$h(\mathbf{x}) = \nu f(\mathbf{x}) + (1 - \nu) 25 x_1 - 0.5 e^{-x_2} I(x_3 > 0.5)$
Change point detector	- Li et al. [26] detector with the 5th Williams et al. [36] statistic	
	- Iguchi et al. [19] - Eigenvector Perturbation Control Chart	
SNR	3, 5	

Table 2: The factor and levels of the simulation study

with multiple predictors. Due to the good performance of the proposed control chart in the first simulation study, the second simulation study aims to identify under what conditions the performance begins to degrade.

4.1 Comparing with other approaches

Here, we describe the details of the simulation study in section 4.1.1 and the corresponding results in section 4.1.2 demonstrating the superior performance of the proposed control chart.

4.1.1 Simulation details

We begin the simulation study by comparing nonlinear nonparametric profile monitoring methods on the profile combinations provided in Iguchi et al.. The factors and levels of the first half of the simulation study are detailed in Table 2. We define the signal-to-noise ratio (SNR) as $\text{Var}(f - h)/\sigma^2$. As we use $\epsilon^t \sim N(0, I)$ for all t , the SNR is simply $\text{Var}(f - h)$. The values of ν in Table 2 were obtained from Iguchi et al where they calibrated $\nu \in (0, 1)$ to achieve a particular SNR.

Li et al. used a smoothing parameter λ in their a EWMA based scheme and performed a sensitivity analysis on this parameter. They observed that ARL_1 becomes shorter as λ becomes smaller. We used the smallest value of $\lambda = 0.05$ that was used in their sensitivity analysis. Li et al. recommended the use of the 2nd, 3rd, or 5th Williams et al. statistic as choices for the statistics on residuals from the SVR. As described in Iguchi et al., the performance of the Li et al. on the profile combinations in Table 2 do not differ greatly in ARL_1 . The choice of using the 5th Williams et al. statistic resulted in the smallest FAR in the simulation study in Iguchi et al. As such, we used the 5th Williams et al. statistic in the Li et al. monitoring approach.

For calibrating control limits using a Monte Carlo approach, control limits were calibrated to a target ARL_0 of 200 or 370 using f explicitly to generate profiles. Each trial in the Monte Carlo approach consisted of randomly generating a set of historical profiles, fitting a model to the historical profiles, and monitoring a sequence of in-control profiles until a false alarm was raised. Control limits were calibrated by finding the smallest observed monitoring statistic that met or exceeded the desired ARL_0 over 390 trials. When the bootstrap approach to setting a control limit is used in the eigenvector perturbation control chart, settings of $\zeta = 10^{-3}$, $c = 10^{-14}$, $N = 1000$, and $N_0 = 5000$ were used.

To estimate the ARL_1 and FAR of each method, 100 trials were conducted for each treatment combination of the factors listed in Table 2. In each trial, m historical profiles were randomly generated and a control limit was either read in from previous calibration attempts via Monte Carlo or obtained by using the m historical profiles (e.g., the bootstrap calibration procedure). Once a control limit was established, monitoring began and a new profile was generated for each time step. If a false alarm occurred, the monitoring procedure was reset and restarted as if monitoring had just begun. The time of the last in-control profile τ was fixed and remained unaffected by the number of false alarms. Monitoring ended when the monitoring procedure raised an alarm after time τ . If $t_{\text{true alarm}, i}$ denotes the time a true alarm occurs for the i th trial, the ARL_1 was estimated by $\frac{1}{100} \sum_{i=1}^{100} (t_{\text{true alarm}, i} - \tau)$. If n_{alarm} denotes the number of false alarms across all 100 trials, the FAR was estimated as $n_{\text{alarm}}/(100 + n_{\text{alarm}})$. This quantity corresponds to the proportion of starts or restarts that end in a false alarm (i.e., the proportion of alarms that are false alarms).

4.1.2 Results

A summary of the results are listed in Table 3. Observe the proposed profile monitoring method using a control limit obtained from bootstrapping outperformed its competitors: the sensitivity of the proposed method is not affected by dramatically increasing the ARL_0 . Lower bounds for the ARL_0 of the eigenvector perturbation control chart using the control limit obtained through bootstrapping are shown in Table 4. The competing methods either cannot calibrate to

Method	ARL_0	τ	Range of observed FAR	Range of observed ARL_1	Fast Calibration?	Unknown f allowable?
Li et al.	200	30	(0.17, 0.37)	(4.24, 4.86)	No	No
	370	30	(0.07, 0.34)	(4.37, 5.39)	No	No
Iguchi et al.	200	30	(0.07, 0.25)	(1, 2.44)	No	No
	370	30	(0.01, 0.11)	(1, 2.75)	No	No
Eigenvector Perturbation	200	30	(0.17, 0.69)	(1, 1)	No	No
	370	30	(0.01, 0.55)	(1, 1)	No	No
	$> 7 \times 10^6$	30	(0, 0)	(1, 1)	Yes	Yes
	$> 7 \times 10^6$	10^4	(0, 0.01)	(1, 1)	Yes	Yes

Table 3: A comparison of nonparametric (or semiparametric) profile monitoring methods with multiple predictors. The profile monitoring methods were used on each treatment of a full-factorial design of the factors and levels listed in Table 2. For each treatment in the computer experiment, 100 trials were used and a FAR and ARL_1 were computed. The noninteger FAR and ARL_1 reported are rounded. We list the range of FAR and ARL_1 across all treatments of the test design. For each treatment in the computer experiment, we recorded the proportion of trials resulting in successful UCL calibration.

such a large ARL_0 or underperform with respect to FAR and ARL_1 . If the Iguchi et al. and Li et al. methods could be calibrated to a $ARL_0 > 7 \times 10^6$, the FAR could certainly be competitive with the eigenvector perturbation control chart. Doing so, however, comes at the cost of increasing ARL_1 as demonstrated by increasing the ARL_0 from 200 to 370. Even at $ARL_0 = 370$, both of these competing methods could not achieve an $ARL_1 = 1$ across all treatments in the computer experiment, while the eigenvector perturbation control chart did achieve this feat. As a low FAR should be expected from setting $\tau = 30$ when a control chart is calibrated to $ARL_0 > 7 \times 10^6$, we increased τ to 10^4 for the proposed method. Even at a large value of τ , the FAR is extremely small. In fact, 13 of 16 treatments resulted in no false alarms. Additionally, as the eigenvector perturbation control chart does not actually estimate the functional relationship between the predictors and the response, it is computationally much faster than its competitors (see Table 5).

In-control profile	m	ARL_0^*	Finished by $T = 10^7$	Lower bound on ARL_0
quadratic	20	3947093	35	7881483
linear	20	2553138	37	7244662
quadratic	40	4362645	29	8365168
linear	40	2815431	52	7068576

Table 4: ARL_0^* of eigenvector perturbation control charts with 10^{-14} quantile trick using equally spaced k_1^* on profiles from Table 2. Due to memory and time constraints, we compute a right censored average run length ARL_0^* taken over runs that raised a false alarm by timestep 10^7 (and excludes runs having no false alarms by timestep 10^7). As the earliest a false alarm could have been raised for the censored trials is $10^7 + 1$, we can place a lower bound on ARL_0 by assuming the censored trials all raised an alarm at time step $10^7 + 1$.

4.2 Investigating the boundaries of "good" performance

We describe the details of the simulation study in section 4.2.1 designed to identify settings where the proposed control chart's performance degrades. The simulation results in section 4.2.2 show how the eigenvector perturbation control chart loses its good performance under conditions which are either the result of windowing, a consequence of monitoring correlations, or a truly difficult where any nonparametric profile monitoring procedure would struggle.

Method	Min	Median	Max
Eigenvector Perturbation	0.000	0.001	0.060
Li et al. [26]	0.021	0.025	0.041
Iguchi et al. [19]	15.452	28.003	41.365

Table 5: Runtimes in seconds for 100 iterations of computing the monitoring statistic from an observed profile and deciding if a profile is in-control or out-of-control. The simulations were conducted under $m = 20$ historical profiles, a window size of $w = 10$ (if applicable), and the profile used for all 100 iterations was the in-control quadratic profile from Table 2, and $m = 20$.

4.2.1 Simulation Details

In the previous subsection, we demonstrated the superior performance of the eigenvector perturbation control chart for the in-control and out-of-control profile combinations listed in Table 2. In this subsection we explore the scenarios where the performance of the eigenvector perturbation control chart degrades and no longer achieves a zero false alarm rate and ARL_1 of one. Additionally, we used the control limits obtained through the bootstrap procedure, which implies the competing methods either cannot calibrate to a similarly large ARL_0 or cannot have the comparable FAR performance. Therefore, we do not consider simulating the competing methods in this setting.

Certainly if $h \propto f$, we should expect the eigenvector perturbation control chart will not be able to detect an out-of-control signal. As such, we consider two other factors in this simulation study. The first is the correlation $\rho(f, h)$ between the in-control and out-of-control functional relationships, f and h , respectively. Additionally, the variance of the sample correlation of two observed in-control profiles depends on the ratio of $\text{Var}(f)$ with respect to the noise σ^2 . So we include $\text{Var} f$ as the second additional factor in the simulation study and hold $\sigma^2 = 1$. Details of the profile calibration methodology can be found in the supplementary materials.

In this subsection we consider profiles where the functional relationships between the response and predictors are zero intercept quadratic polynomials. That is, we assume f, g , and h are of the following form:

$$f(\mathbf{x}) = \mathbf{x}^\top \mathbf{A} \mathbf{x} + \mathbf{a}^\top \mathbf{x}, \quad g(\mathbf{x}) = \mathbf{x}^\top \mathbf{B} \mathbf{x} + \mathbf{b}^\top \mathbf{x}, \quad \text{and} \quad h(\mathbf{x}) = \nu f(\mathbf{x}) + (1 - \nu)g(\mathbf{x})$$

where $\mathbf{A}, \mathbf{B} \in \mathbb{R}^{d \times d}$, $\mathbf{a}, \mathbf{b} \in \mathbb{R}^d$ and ν is an affine combination parameter. If $\nu \in (0, 1)$, then h is a convex combination of f and g . Otherwise, h is a nonconvex combination of f and g . We additionally constrain g such that $\text{Cov}(f, g) = 0$ to ease profile calibration efforts and improve interpretability of the results. Observe if $\nu < 0$, then $\rho(f, h) < 0$. As we want to consider difficult cases for the eigenvector perturbation control chart we will ignore the scenario where $\nu < 0$. The factors and levels of the simulation study are outlined in Table 6.

Recall from Section 3.2, that the eigenvector perturbation of $\mathbb{E} \mathbf{R}$ is a function of γ_1, γ_{12} , and γ_2 . Although these are biased estimates of their population counterparts, they converge to the population correlation as $n \rightarrow \infty$. As such, we provide an illustration for the population correlations for two in-control profiles $\rho(f + \epsilon_1, f + \epsilon_2)$, for an in-control profiles and an out-of-control profile $\rho(f + \epsilon_1, h + \epsilon_2)$, and for two out-of-control profiles $\rho(h + \epsilon_1, h + \epsilon_2)$ for all possible profile combinations in Table 6, where $\epsilon_1, \epsilon_2 \in \mathbb{R}$ are noise independent of each other and of the predictors \mathbf{x} . The quantities are computed as

$$\rho(f + \epsilon_1, f + \epsilon_2) = \frac{\text{Var}(f)}{\text{Var}(f) + \sigma^2}, \quad \rho(h + \epsilon_1, h + \epsilon_2) = \frac{\text{Var}(h)}{\text{Var}(h) + \sigma^2},$$

and

$$\rho(f + \epsilon_1, h + \epsilon_2) = \frac{\text{Cov}(f, h)}{\sqrt{\text{Var}(f) + \sigma^2} \sqrt{\text{Var}(h) + \sigma^2}} = \rho(f, h) \rho(f + \epsilon_1, f + \epsilon_2)^{1/2} \rho(h + \epsilon_1, h + \epsilon_2)^{1/2}$$

where the last equality is obtained through repeated uses of the definition of correlation.

Factor	Level
τ	0, 30, 10^4
n	128, 256, 512
m	20, 40
m/w	1, 2
SNR	3, 5
$\text{Var}(f)$	2, 4, 6
$\rho(f, h)$	0.75, 0.9
convexity of h with respect to f and g	convex, non-convex combinations

Table 6: The factors and levels for the simulation study on the eigenvector perturbation control chart using quadratic polynomials for the in-control and out-of-control profiles. All possible treatment combinations were implemented. Note certain combinations of $\text{Var}(f)$, SNR, $\rho(f, h)$ and choice of convexity cannot be achieved.

For the simulation study, \mathbf{X} was randomly chosen from $\text{Unif}([0, 1]^{25})$ at the beginning of each trial and held fixed for all time steps t . The eigenvector perturbation control chart used the same values of ζ, c, N , and N_0 as in Section 4.1. For each treatment condition, 100 trials were conducted. The noise in each profile were sampled independently from $N(0, 1)$. The calculations of the sample FAR and ARL_1 were the same as in Section 4.1.

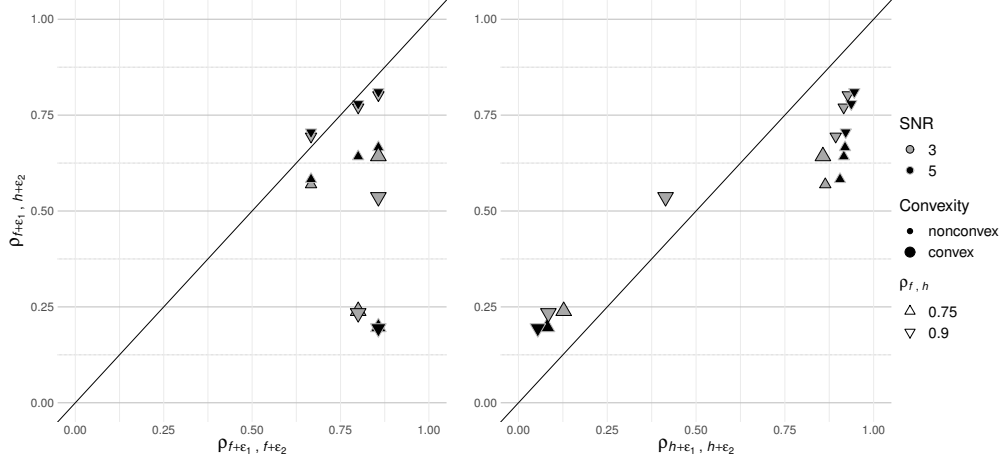


Figure 2: A visualization of the population correlation between profile combinations in Table 6. Each point corresponds to a particular treatment combination of an in-control profile and an out-of-control profile in Table 6

4.2.2 Results

Figure 3 shows the sample FAR across the factors in Table 6 which influence in-control performance. As expected, the sample FAR for $\tau = 30$ was zero in all but one case. When $\tau = 10^4$, we observe excellent performance when $n = 512$. Also notice as m/w increased, the FAR decreased. Finally, as $\text{Var}(f)$ increased with n fixed, the FAR tended to decrease. Therefore, a practitioner can decrease the FAR by increasing n , m , m/w , and, if possible, $\text{Var}(f)/\sigma^2$.

Figure 4 depicts the sample ARL_1 across the factors in Table 6 which influence out-of-control performance. As expected, ARL_1 decreased with increasing n , m/w , or $\rho(f, h)$. There is a counterintuitive result: the ARL_1 did not decrease uniformly with increasing SNR and $\text{Var}(f)$ (e.g., $\text{Var}(f) = 4$). This curious result is explained by considering the correlation between *profiles* as opposed to the correlation between in-control and out-of-control functions f and h . As Figure 2 shows, the out-of-control profiles obtained through a nonconvex combination of f and g tend to have $\rho(f + \epsilon_1, f + \epsilon_2) \approx \rho(f + \epsilon_1, h + \epsilon_2)$. In fact, the closer these two quantities are, the larger the ARL_1 . It seems the only reason the eigenvector perturbation control chart is able to detect an out-of-control profile is due to the difference between $\rho(h + \epsilon_1, h + \epsilon_2)$ and $\rho(f + \epsilon_1, h + \epsilon_2)$. This scenario should be difficult for any control chart that monitors correlations.

As the variability of the sample correlation increases with decreasing n , we should expect poor performance when small n is combined with nonconvex combinations of f and g along with a large $\rho(f, h)$. For example, in the $n = 64$ case with $\rho(f, h) = 0.9$, $\text{Var}(f) < 6$, and $\nu > 1$, 15 trials of 4800 trials across the relevant 48 treatment combinations from Table 6 failed to raise an alarm by time $t = 10500$.

In addition to simulating the performance of the proposed control chart under large correlations, we also performed simulations for smaller and negative correlations (with $\rho(f, h) \in \{-1, -0.75, -0.5, -0.3, 0, 0.3, 0.5\}$) and varied all other factors listed in Table 6. For all of these additional settings of $\rho(f, h)$, the control chart demonstrated optimal performance with $ARL_1 = 1$.

5 Discussion

We established a new nonparametric profile monitoring technique using eigenvector perturbation. The profile monitoring literature typically calibrates control limits to ARL_0 of 200 or 370. For nonparametric profile monitoring methods, a Monte Carlo approach is commonly required to calibrate control limits. For such approaches, calibrating to extremely large ARL_0 on the order of 10^6 is infeasible and impractical. The proposed profile monitoring method is able to quickly calibrate to a $ARL_0 > 10^6$. For a general control chart, the ARL_0 increases the ARL_1 tends to increase as well. Despite such a large ARL_0 , the eigenvector perturbation control chart does not suffer much loss in terms of ARL_1 even when $\tau = 10^4$. The performance of the eigenvector perturbation control chart degrades under truly difficult situations. The FAR increases when the correlation between in-control profiles is unstable (i.e., $\text{Var}(f) \approx \sigma^2$ or n small), and the ARL_1 increases when there is little change in the correlation structure between profiles.

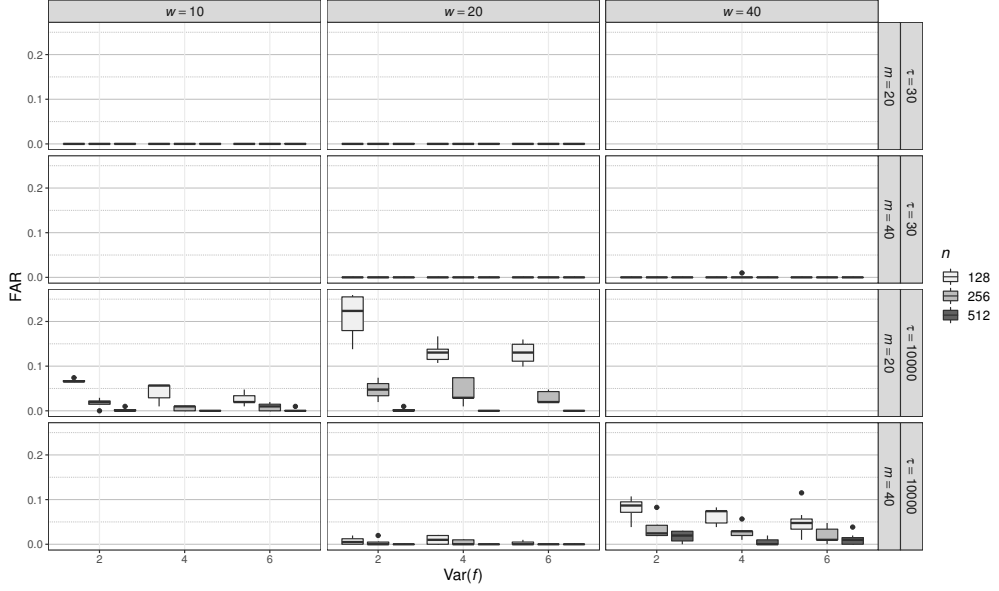


Figure 3: Boxplots of the false alarm rates for the eigenvector perturbation control chart for the simulation study detailed in Table 6. For each treatment combination listed in Table 6, 100 trials were performed and a sample FAR was computed. Each boxplot is drawn using the sample FARs across the various choices of SNR, $\rho(f, h)$, and choice of convex combination of f and h , as these quantities affect alarms after τ and do not affect the FAR. Whenever the illustrated boxplots are flat with no outliers, zero false alarms were observed. Conditions not detailed in Table 6 result in empty plots.

The areas for future work and extensions are plentiful. First, the eigenvector perturbation control chart works solely off of the noisy responses of a profile. The current control chart could be extended by measuring the correlation of some aspect of fitted profiles. Many profile monitoring methods apply a multivariate control chart to some fitted parameter for f . This could be done with the eigenvector perturbation control chart as well. For example, the weights in a basis function expansion of f in the $d = 1$ setting could be used in place of noisy responses. The traditional approach of applying a multivariate control chart to fitted parameters can lead to issues especially if there are underlying problems with identifiability with the fitted model.

The eigenvector perturbation control chart may provide a different approach if applied to fitted or predicted values instead of noisy responses (say $\hat{y}_i = f(\mathbf{x}_i) + (\hat{y}_i - f(\mathbf{x}_i)) = f(\mathbf{x}_i) + \eta_i$). Recall the FAR and ARL_1 tended to perform better as $Var(f)/\sigma$ increased. If fitted values were to be used, we could expect similar good performance when $Var(f)/Var(f - \hat{f})$ is large. That is, if extended to work on fitted values, the eigenvector perturbation control chart performance could increase as the fit of f gets better.

There are inherent weaknesses with the eigenvector perturbation control chart that could be improved upon: monitoring something other than correlations and allowing for predictors to change over time. As the current form of the control chart monitors correlations, future work may include a control chart that also monitors if $\nu = 1$ in addition to monitoring correlations. Lastly, the current approach is restrictive in its assumption that the predictors are fixed for all time steps t . Approaches to loosen this assumption could include replacing the traditional sample correlation with a rank based correlation statistic or using predicted values $\hat{f}(\mathbf{X})$ where \mathbf{X} and the estimation procedure are chosen to give good predictions for some $\mathbf{X}^t \neq \mathbf{X}$.

Disclaimer

The views expressed in this article are those of the author and do not reflect the official policy or position of the United States Air Force, Department of Defense, or the U. S. Government.

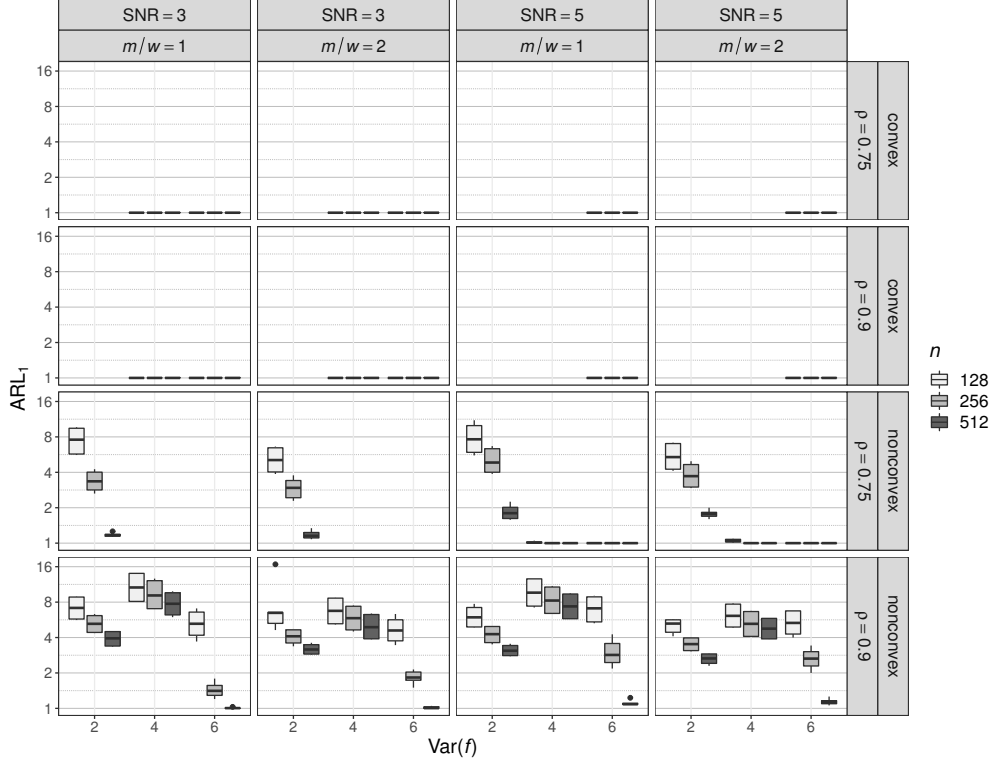


Figure 4: Boxplots of the ARL_1 for the eigenvector perturbation control chart for the simulation study detailed in Table 6. For each treatment combination listed in Table 6, 100 trials were performed and a sample ARL_1 was computed. Each boxplot is drawn using the sample ARL_1 across the various choices of τ and m as τ . We omit these factors as facets in the facet plot as τ has little effect on ARL_1 , and although m has some effect on ARL_1 , we do not include for sake of clarity. Whenever the illustrated boxplots are flat with no outliers, $ARL_1 = 1$ in all cases.

Acknowledgments

This research was supported by the Office of the Secretary of Defense, Directorate of Operational Test and Evaluation, and the Test Resource Management Center under the Science of Test research program (FA8075-14-D-0019/FA807518F1525).

References

- [1] Azmy S. Ackleh, Edward James Allen, R. Baker Kearfott, and Padmanabhan Seshaiyer. *Classical and modern numerical analysis*. Chapman and Hall/CRC, July 2009.
- [2] Amirhossein Amiri, Willis A Jensen, and Reza Baradaran Kazemzadeh. A case study on monitoring polynomial profiles in the automotive industry. *Quality and Reliability Engineering International*, 26(5):509–520, Oct 2009.
- [3] Shing I. Chang and Srikanth Yadama. Statistical process control for monitoring non-linear profiles using wavelet filtering and B-spline approximation. *International Journal of Production Research*, 48(4):1049–1068, 2010.
- [4] Yuxin Chen, Chen Cheng, and Jianqing Fan. Asymmetry helps: eigenvalue and eigenvector analyses of asymmetrically perturbed low-rank matrices. *The Annals of Statistics*, 49(1):435–458, Feb 2021.
- [5] Eric Chicken, Joseph J. Pignatiello, and James R. Simpson. Statistical process monitoring of nonlinear profiles using wavelets. *Journal of Quality Technology*, 41(2):198–212, 2009.
- [6] Eric Chicken, Raymond Hill, and Joseph J. Pignatiello. Statistical functional process monitoring using clustered data. *67th Annual Conference and Expo of the Institute of Industrial Engineers 2017*, (1):603–608, 2017.
- [7] Shih-Chung Chuang, Ying-Chao Hung, Wen-Chi Tsai, and Su-Fen Yang. A framework for nonparametric profile monitoring. *Computers & Industrial Engineering*, 64:482–491, 2013.

- [8] Bianca M Colosimo, Quirico Semeraro, and Massimo Pacella. Statistical process control for geometric specifications: on the monitoring of roundness profiles. *Journal of Quality Technology*, 40(1):1–18, jan 2008.
- [9] Chandler Davis and W M Kahan. The rotation of eigenvectors by a perturbation. III*. 7(1), 1970.
- [10] Justin Eldridge, Mikhail Belkin, and Yusu Wang. Unperturbed: spectral analysis beyond Davis-Kahan. In *Proceedings of Algorithmic Learning Theory*, volume 83 of *Proceedings of Machine Learning Research*, pages 321–358. PMLR, 2018.
- [11] Jianqing Fan, Weichen Wang, and Yiqiao Zhong. An ℓ_∞ eigenvector perturbation bound and its application. *Journal of Machine Learning Research*, 18(207):1–42, 2018.
- [12] R. A. Fisher. Frequency distribution of the values of the correlation coefficient in samples from an indefinitely large population. *Biometrika*, 10(4):507–521, 1915.
- [13] M.M. Gardner, Jye-Chyi Lu, R.S. Gyurcsik, J.J. Wortman, B.E. Hornung, H.H. Heinisch, E.A. Rying, S. Rao, J.C. Davis, and P.K. Mozumder. Equipment fault detection using spatial signatures. *IEEE Transactions on Components, Packaging, and Manufacturing Technology: Part C*, 20(4):295–304, 1997.
- [14] Marco Grasso, Alessandra Menafoglio, Bianca M. Colosimo, and Piercesare Secchi. Using curve-registration information for profile monitoring. *Journal of Quality Technology*, 48(2):99–127, 2016.
- [15] Peter Hackl and Johannes Ledolter. A control chart based on ranks. *Journal of Quality Technology*, 23(2):117–124, 1991.
- [16] Zahra Hadidoust, Yaser Samimi, and Hamid Shahriari. Monitoring and change-point estimation for spline-modeled non-linear profiles in phase II. *Journal of Applied Statistics*, 42(12):2520–2530, 2015.
- [17] Ying Chao Hung, Wen Chi Tsai, Su Fen Yang, Shih Chung Chuang, and Yi Kuan Tseng. Nonparametric profile monitoring in multi-dimensional data spaces. *Journal of Process Control*, 22(2):397–403, 2012.
- [18] Takayuki Iguchi, Dustin G Mixon, Jesse Peterson, and Soledad Villar. Probably certifiably correct k -means clustering. *Math. Program., Ser. A*, 165:605–642, 2017.
- [19] Takayuki Iguchi, Andrés F. Barrientos, Eric Chicken, and Debajyoti Sinha. Nonlinear profile monitoring with single index models. *Quality and Reliability Engineering International*, 37(7):3004–3017, 2021.
- [20] Michael Imhoff and Silvia Kuhls. Alarm algorithms in critical care monitoring. *Anesthesia & Analgesia*, 102(5):1525–1537, May 2006.
- [21] Jionghua Jin and Jianjun Shi. Feature-preserving data compression of stamping tonnage information using wavelets. *Technometrics*, 41(4):327–339, nov 1999.
- [22] Lan Kang and Susan L Albin. On-line monitoring when the process yields a linear profile. *Journal of Quality Technology*, 32(4):418–426, oct 2000.
- [23] Arun Kuchibhotla and Rohit Patra. Efficient estimation in single index models through smoothing splines. *Bernoulli*, 26(2):1587–1618, 2020.
- [24] Arun Kumar Kuchibhotla and Rohit Kumar Patra. *simest: single index model estimation with constraints on link function*, 2017. R package version 0.4.
- [25] Erich L Lehmann and George Casella. *Theory of point estimation*. Springer Science & Business Media, 2006.
- [26] Chung I. Li, Jeh Nan Pan, and Chun Han Liao. Monitoring nonlinear profile data using support vector regression method. *Quality and Reliability Engineering International*, 35(1):127–135, 2019.
- [27] Kelly McGinnity, Eric Chicken, and Joseph J. Pignatiello. Nonparametric changepoint estimation for sequential nonlinear profile monitoring. *Quality and Reliability Engineering International*, 31(1):57–73, 2015.
- [28] David Morales-Jimenez, Iain M Johnstone, Matthew R McKay, and Jeha Yang. Asymptotics of eigenstructure of sample correlation matrices for high-dimensional spiked models. *Statistica Sinica*, 31(2):571, 2021.
- [29] Mehrdad Nikoo and Rassoul Noorossana. Phase II monitoring of nonlinear profile variance using wavelet. *Quality and Reliability Engineering International*, 29(7):1081–1089, 2013.
- [30] Gabriel J. Odom, Kathryn B. Newhart, Tzahi Y. Cath, and Amanda S. Hering. Multistate multivariate statistical process control. *Applied Stochastic Models in Business and Industry*, 34(6):880–892, 2018.
- [31] Sean O'Rourke, Van Vu, and Ke Wang. Random perturbation of low rank matrices: improving classical bounds. *Linear Algebra and Its Applications*, 540:26–59, nov 2013.
- [32] Jyh-Jen Horng Shiau, Hsiang-Ling Huang, Shuo-Hui Lin, and Ming-Ye Tsai. Monitoring nonlinear profiles with random effects by nonparametric regression. *Communications in Statistics - Theory and Methods*, 38(10):1664–1679, 2009.

- [33] Roumen Varbanov, Eric Chicken, Antonio Linero, and Yun Yang. A Bayesian approach to sequential monitoring of nonlinear profiles using wavelets. *Quality and Reliability Engineering International*, 35(3):761–775, 2019.
- [34] Tengyao Wang and Richard J Samworth. High dimensional change point estimation via sparse projection. *J. R. Statist. Soc. B*, 80:57–83, 2018.
- [35] Yuan Wang, Yajun Mei, and Kamran Paynabar. Thresholded multivariate principal component analysis for phase I multichannel profile monitoring. *Technometrics*, 60(3):360–372, 2018.
- [36] James D. Williams, William H. Woodall, and Jeffrey B. Birch. Statistical monitoring of nonlinear product and process quality profiles. *Quality and Reliability Engineering International*, 23(8):925–941, dec 2007.
- [37] William H. Woodall and Frederick W. Faltin. Rethinking control chart design and evaluation. *Quality Engineering*, 31(4):596–605, 2019.
- [38] Wenwan Yang, Changliang Zou, and Zhaojun Wang. Nonparametric profile monitoring using dynamic probability control limits. *Quality and Reliability Engineering International*, 33(5):1131–1142, 2017.
- [39] Yi Yu, Tengyao Wang, and Richard J. Samworth. A useful variant of the Davis–Kahan theorem for statisticians. *Biometrika*, 102(2):315–323, may 2014.
- [40] Changliang Zou, Peiha Qiu, and Douglas Hawkins. Nonparametric control chart for monitoring profiles using change point formulation and adaptive smoothing. *Statistica Sinica*, 19(3):1337–1357, 2009.